# Expanded View Figures

**Figure EV1. *Listeria monocytogenes* infection induces LLO-dependent ER redistribution and NMHCIIA–Gp96 interaction.**

A Flow cytometry analysis of surface-exposed Gp96 levels in HeLa cells left uninfected (U) or infected with wt or Δ*hly Lm* for 1 h. Values are mean ± SEM ($n \geq 3$), and *P*-values were calculated using one-way ANOVA with Tukey's *post hoc* analyses, $^{**}P < 0.01$

B Confocal microscopy images of HeLa cells left uninfected or infected with wt or Δ*hly Lm* for 1 h, fixed and immunolabelled for ER-KDEL (green) and Gp96 (red) and stained with DAPI (blue). Insets show ER-Gp96 vacuoles. Arrows indicate ER-KDEL vacuoles. Scale bars, 10 μm.

C Confocal microscopy images of HeLa cells left untreated or treated with the indicated concentrations of LLO for 15 min, fixed and immunolabelled for ER-KDEL (green) and stained with DAPI. Arrows indicate ER-KDEL vacuoles. Scale bars, 10 μm.

D Confocal microscopy images of HeLa cells left untreated or treated with 0.5 nM LLO for 15 min and immunolabelled for Gp96 (red) and ER-KDEL (green). Arrows indicate ER-Gp96 vacuoles shown enlarged in the insets 1 and 2. Scale bars, 10 μm.

E TEM images of HeLa cells left untreated or treated with 0.5 nM LLO for 15 min. Arrowheads indicate normal ER cisternae, and arrows show ER vacuoles at the proximity of PM.

F Flow cytometry analysis of surface-exposed Gp96 levels in HeLa cells left untreated (U) or treated with 0.5 nM LLO for 15 min. Values are mean ± SEM ($n \geq 3$), and *P*-values were calculated using two-tailed unpaired Student's *t*-test, $^{*}P < 0.05$

G Amino acid sequence of the human NMHCIIA with functional domains indicated. Peptide sequences recovered from MS/MS are highlighted in red.

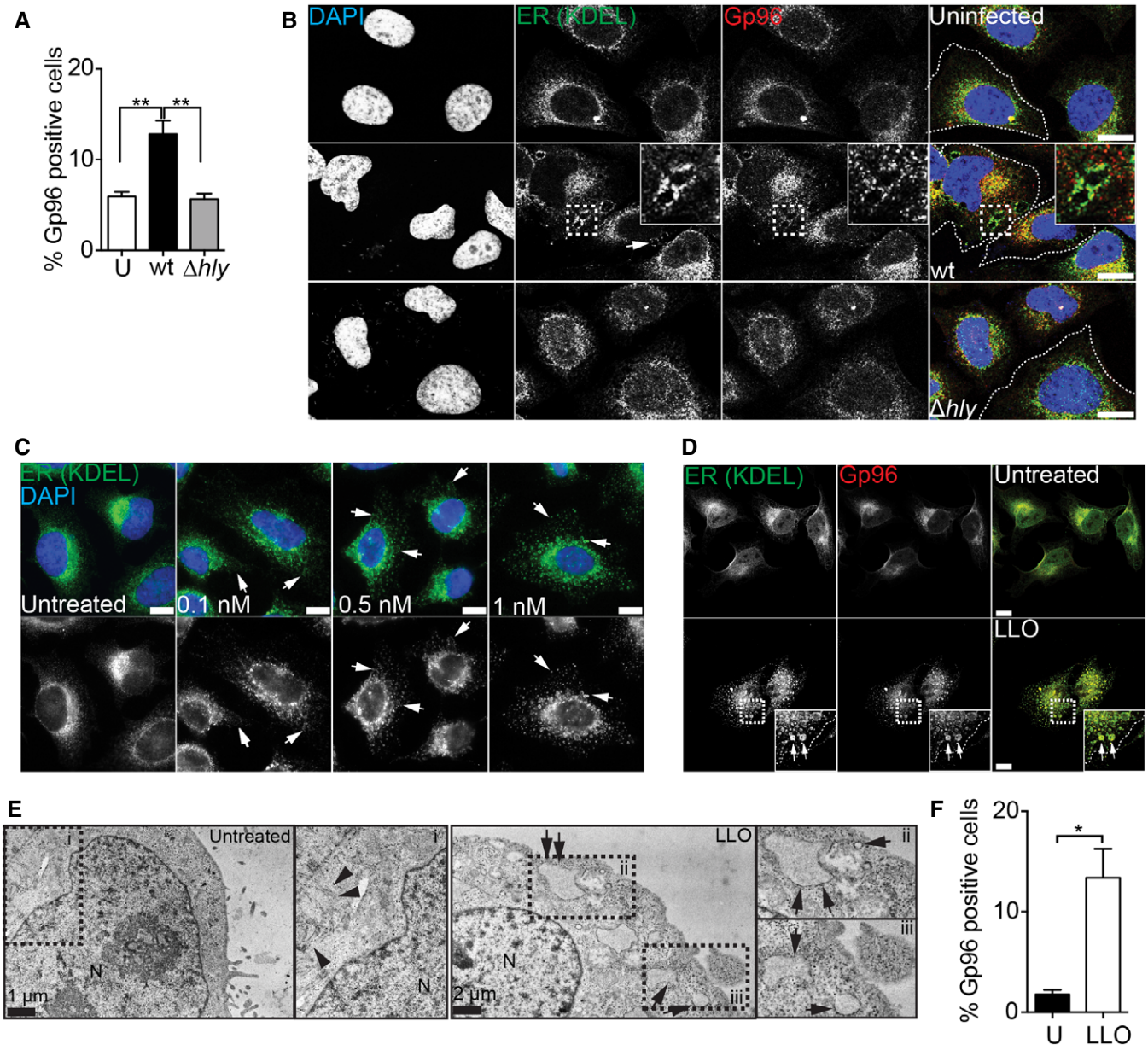


G

```
1    MAQQAADKYLYVDKNFINNPLAQADWAAKKLVWVPSDKSGFEPASLKEEVGEEAIVELVENGKKVKVNKDDIQKMNPPKFSKVEDMAELTCLNEASVLHN
101  LKERYYSGLIYTYSGLFCVVINPYKNLPIYSEEIVEMYKGKKRHEMPPHIYAITDTAYRSMMQDREDQSILCTGESGAGKTENTKKVIQYLAYVASSHKS
201  KKDQGELERQLLQANPILEAFGNAKTVKNDNSSRFGKFIRINFDVNGYIVGANIETYLLEKSRAIRQAKEERTFHIFYYLLSGAGEHLKTDLLLEPYNKY
301  RFLSNGHVTIPGQQDKDMFQETMEAMRIMGIPEEEQMGLLRVISGVLQLGNIVFKKERNTDQASMPDNTAAQKVSHLLGINVTDFTRGILTPRIKVGRDY
401  VQKAQTKEQADFAIEALAKATYERMFRWLVLRINKALDKTKRQGASFIGILDIAGFEIFDLNSFEQLCINYTNEKLQQLFNHTMFILEQEEYQREGIEWN
501  FIDFGLDLQPCIDLIEKPAGPPGILALLDEECWFPKATDKSFVEKVMQEQGTHPKFQKPKQLKDKADFCIIHYAGKVDYKADEWLMKNMDPLNDNIATLL
601  HQSSDKFVSELWKDVDRIIGLDQVAGMSETALPGAFKTRKGMFRTVGQLYKEQLAKLMATLRNTNPNFVRCIIPNHEKKAGKLDPHLVLDQLRCNGVLEG
701  IRICRQGFPNRVVFQEFRQRYEILTPNSIPKGFMDGKQACVLMIKALELDSNLYRIGQSKVFFRAGVLAHLEEERDLKITDVIIGFQACCRGYLARKAFA
801  KRQQQLTAMKVLQRNCAAYLKLRNWQWWRLFTKVKPLLQVSRQEEEMMAKEEELVKVREKQLAAENRLTEMETLQSQLMAEKLQLQEQLQAETELCAEAE
901  ELRARLTAKKQELEEICHDLEARVEEEEERCQHLQAEKKMQQNIQELEEQLEEEESARQKLQLEKVTTEAKLKKLEEEQIILEDQNCKLAKEKKLLEDR
1001 IAEFTTNLTEEEEKSKSLAKLKNKHEAMITDLEERLRREEKQRQELEKTRRKLEGDSTDLSDQIAELQAQIAELKMQLAKKEEELQAALARVEEEAAQKN
1101 MALKKIRELESQISELQEDLESERASRNKAEKQKRDLGEELEALKTELEDTLDSTAAQQELRSKREQEVNILKKTLEEEAKTHEAQIQEMRQKHSQAVEE
1201 LAEQLEQTKRVKANLEKAKQTLENERGELANEVKVLLQGKGDSEHKRKKVEAQLQELQVKFNEGERVRTELADKVTKLQVELDNVTGLLSQSDSKSSKLT
1301 KDFSALESQLQDTQELLQEENRQKLSLSTKLKQVEDEKNSFREQLEEEEEAKHNLEKQIATLHAQVADMKKKMEDSVGCLETAEEVKRKLQKDLEGLSQR
1401 HEEKVAAYDKLEKTKTRLQQELDDLLVDLDHQRQSACNLEKKQKKFDQLLAEEKTISAKYAEERDRAEAEAREKETKALSLARALEEAMEQKAELERLNK
1501 QFRTEMEDLMSSKDDVGKSVHELEKSKRALEQQVEEMKTQLEELEDELQATEDAKLRLEVNLQAMKAQFERDLQGRDEQSEEKKKQLVRQVREMEAELED
1601 ERKQRSMAVAARKKLEMDLKDLEAHIDSANKNRDEAIKQLRKLQAQMKDCMRELDDTRASREEILAQAKENEKKLKSMEAEMIQLQEELAAAERAKRQAQ
1701 QERDELADEIANSSGKGALALEEKRRLEARIAQLEEELEEEQGNTELINDRLKKANLQIDQINTDLNLERSHAQKNENARQQLERQNKELKVKLQEMEGT
1801 VKSKYKASITALEAKIAQLEEQLDNETKERQAACKQVRRTEKKLKDVLLQVDDERRNAEQYKDQADKASTRLKQLKRQLEEAEEEAQRANASRRKLQREL
1901 EDATETADAMNREVSSLKNKLRRGDLPFVVPRRMARKGAGDGSDEEVDGKADGAEAKPAE
```

Head domain 1-836

Coiled coil neck and tail domain 837 - 1,960

**Figure EV1.**

**Figure EV2. NMHCIIA–Gp96 interaction and association at cortical structures in HeLa, Caco-2 and RAW 264.7 cells infected with *Listeria monocytogenes* or treated with LLO.**

A–D Immunoblots of NMHCIIA and Gp96 levels from whole-cell lysates (WCL) and (A) NMHCIIA IP or (B–D) Gp96 IP fractions from (A, B) HeLa cells, (C) Caco-2 cells or (D) RAW264.7 macrophages left uninfected (U) or infected with wt *Lm* for 1 h, probed with anti-Gp96 and anti-NMHCIIA antibodies. (A, B) Control IP was carried out using unspecific isotype antibodies ($IgG^{iso}$).

E Confocal microscopy images of Caco-2 cells left untreated or treated with 0.5 nM LLO for 15 min, immunolabelled for NMHCIIA (green) and Gp96 (red) and stained with DAPI (blue). Arrows indicate Gp96-positive NMHCIIA cortical structures. Scale bars, 10 μm.

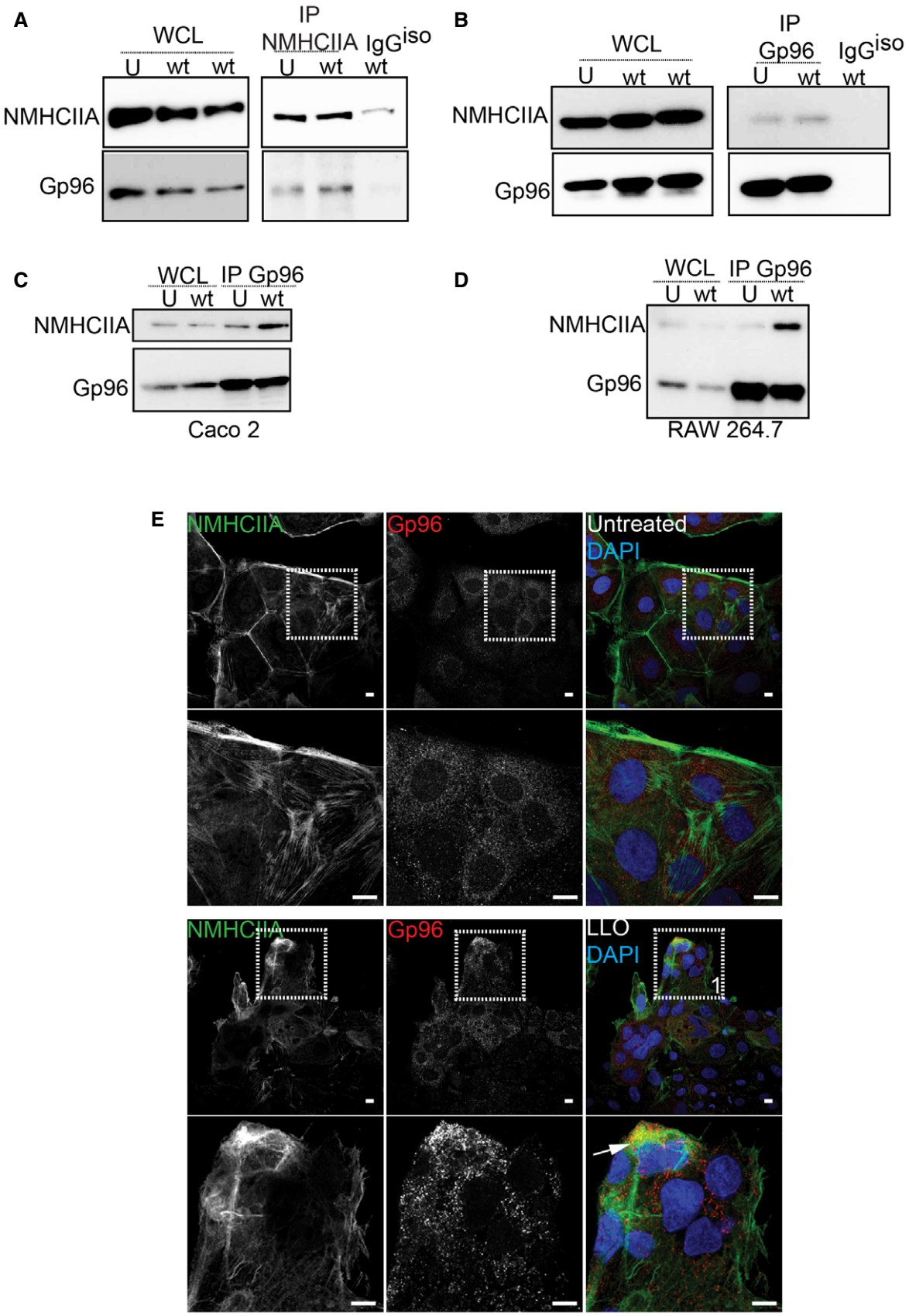


**Figure EV2.**

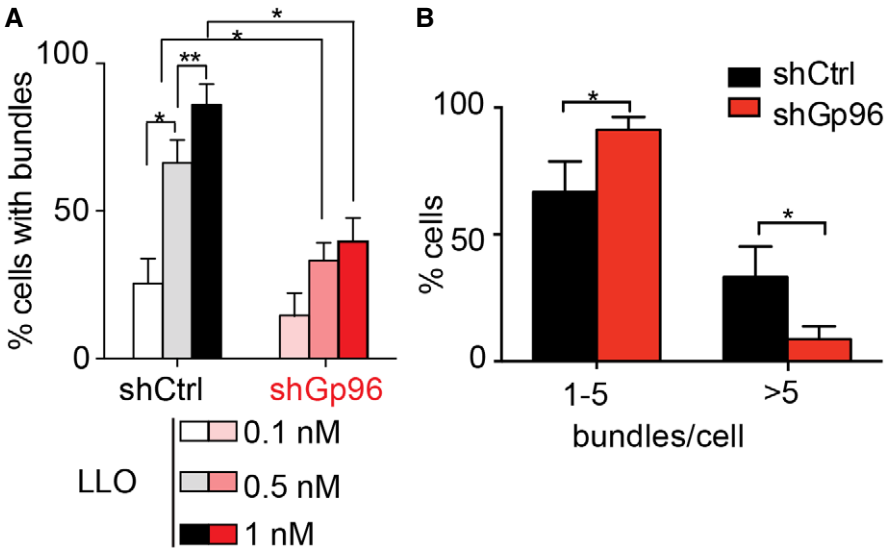


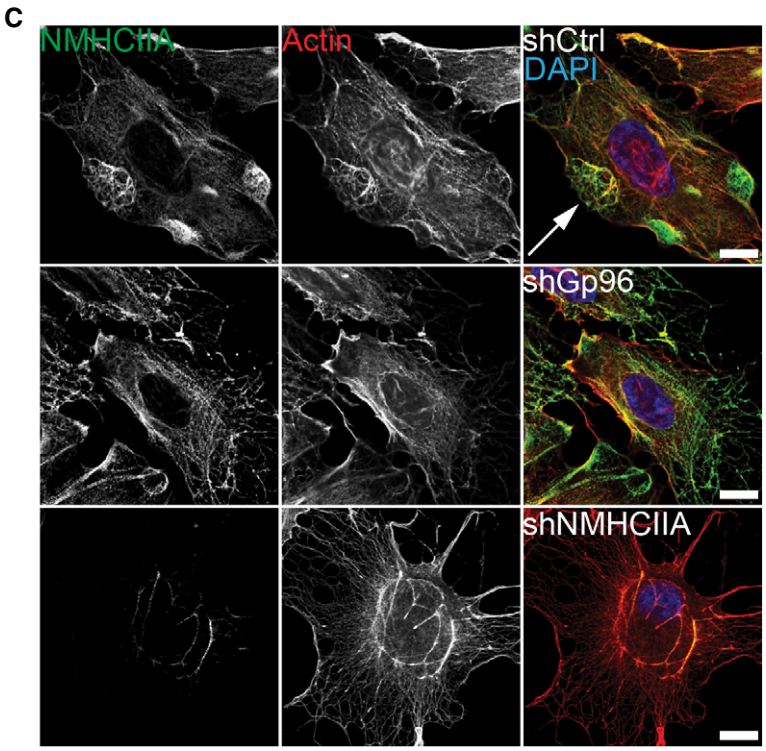


**Figure EV3. Gp96 and NMHCIIA control actomyosin remodelling during LLO treatment.**

A Quantification of the percentage of shControl and shGp96 HeLa cells harbouring NMHCIIA bundles in response to increasing concentrations of LLO.

B Quantification of the percentage of shCtrl and shGp96 HeLa cells harbouring at least 1–5 or > 5 NMHCIIA bundles per cell in response to 0.5 nM LLO (15 min).

C Confocal images of shCtrl, shGp96 or shNMHCIIA HeLa cells treated with 0.5 nM LLO for 15 min and immunolabelled for NMHCIIA (green) and stained with phalloidin (actin, red) and DAPI (blue). Arrow indicates compact actomyosin cortical bundle. Scale bars, 10 μm.

Data information: For all quantifications, values are mean ± SEM ($n \geq 3$) and *P*-values were calculated using one-way ANOVA with Tukey's *post hoc* analyses, $^{*}P < 0.05$, $^{**}P < 0.01$.

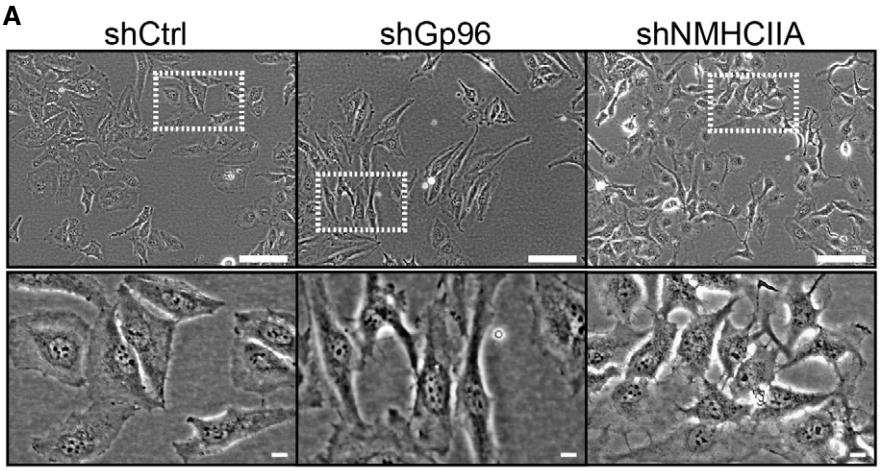


**Figure EV4. Gp96 and NMHCIIA modulate cell shape.**

A Brightfield images of the indicated unfixed HeLa cell lines used for analysis of shape indicators. Scale bars: 100 and 10 μm for top and bottom panels, respectively.

B Quantification of cellular shape indicators. Each point represents one individual cell imaged and analysed for each parameter in each sample. At least 190 cells were analysed. *P*-values were calculated using one-way ANOVA with Tukey's *post hoc* analyses, *$P < 0.05$, ***$P < 0.001$.

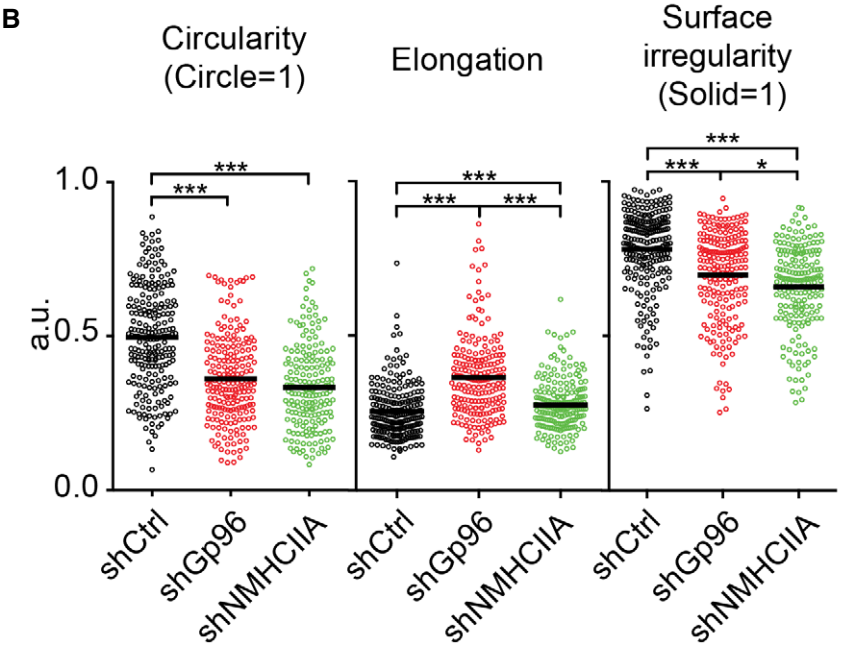


**Figure EV5. Zebrafish is a valuable model to study the cell biology of *Lisateria monocytogenes* infection.**

A CFU counts per zebrafish larva infected with various doses (low, medium and high) of wt *Lm* at different times post-infection. Results are mean ± SEM ($n \geq 3$) (horizontal bars); each point represents one larva.

B Survival curves of zebrafish larvae infected with different doses (low, medium and high) of wt or Δ*hly Lm*. Values are mean ± SEM ($n \geq 3$) and include a total of $n = 28$ larvae per condition.

C Interaction between *Lm* (GFP, green) and macrophages (Mpeg1-mCherry, red). Sequential frames of time-lapse microscopy analysis of transgenic zebrafish larvae infected in the hindbrain ventricle with a low-dose GFP-expressing *Lm* for 12 h ($t_0$). Scale bars, 20 μm.

D Confocal microscopy images of wt zebrafish larvae infected (low dose) in the tail muscle with the GFP-expressing wt *Lm* for 24 h, stained with phalloidin (actin, red) and DAPI (blue). Insets show *in vivo* actin comet tails. Scale bar, 10 μm.

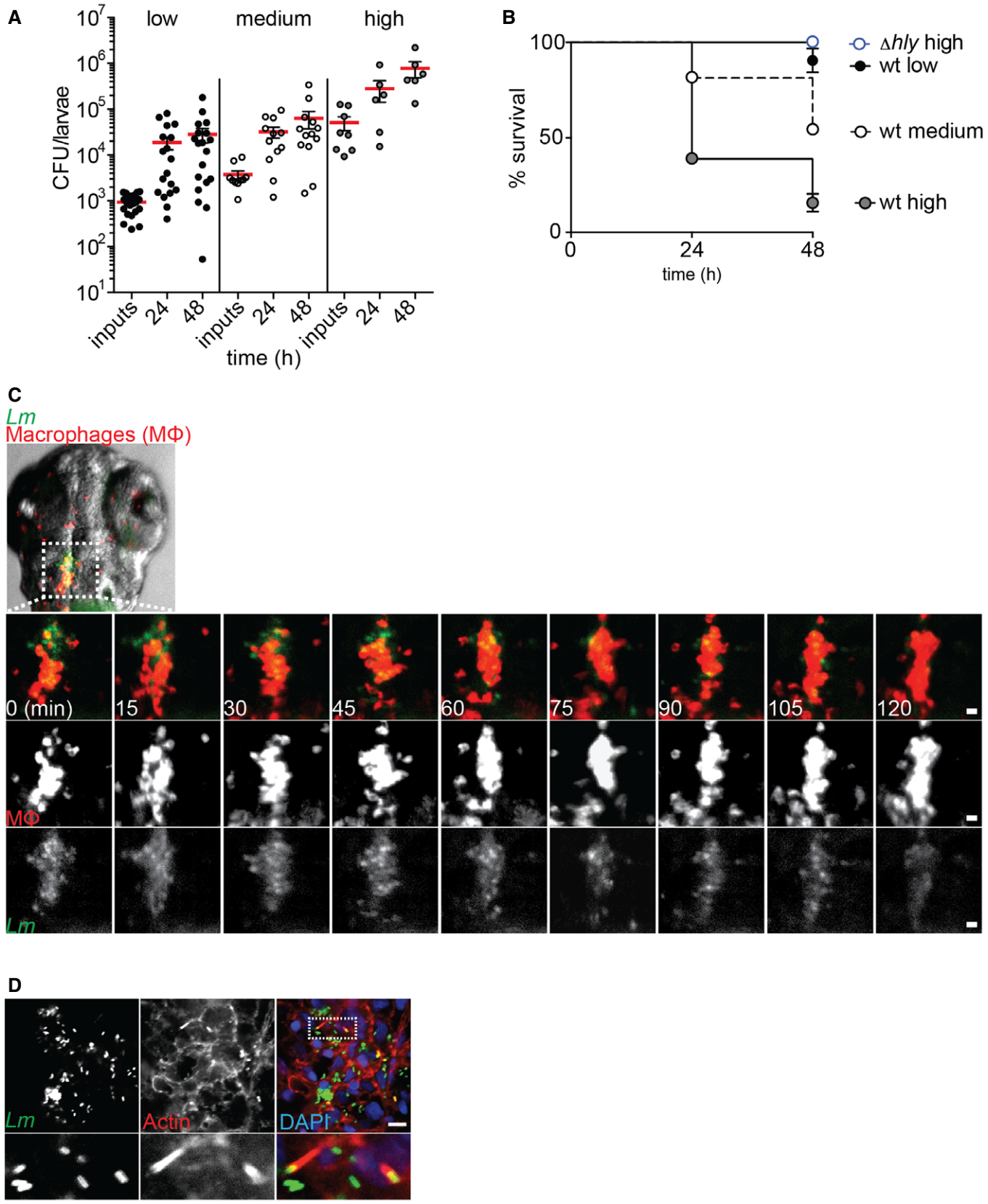
A
low
medium
high
CFU/larvae
inputs
24
48
time (h)
B
% survival
time (h)
Δhly high
wt low
wt medium
wt high
C
Lm
Macrophages (MΦ)
0 (min)
15
30
45
60
75
90
105
120
MΦ
Lm
D
Lm
Actin
DAPI

**Figure EV5.**